Structural properties and photoluminescence of ZnO nanowalls prepared by two-step growth with oxygen-plasma-assisted molecular beam epitaxy

2005 J. Phys.: Condens. Matter 17 3035

(http://iopscience.iop.org/0953-8984/17/19/017)

INSTITUTE OF PHYSICS PUBLISHING JOURNAL OF PHYSICS: CONDENSED MATTER

J. Phys.: Condens. Matter **17** (2005) 3035–3042 doi:10.1088/0953-8984/17/19/017

Structural properties and photoluminescence of ZnO nanowalls prepared by two-step growth with oxygen-plasma-assisted molecular beam epitaxy

X H Zhang[1], Y C Liu[1,4], X H Wang[2], S J Chen[1], G R Wang[1], J Y Zhang[3], Y M Lu[3], D Z Shen[3] and X W Fan[3]

[1] Centre for Advanced Optoelectronic Functional Material Research, Northeast Normal University, Renmin Street 5268, Changchun 130024, People's Republic of China
[2] Key Laboratory of Excited State Processes, Changchun Institute of Optics, Fine Mechanics and Physics, Chinese Academy of Sciences, 16 East South Lake Avenue, Changchun 130021, People's Republic of China
[3] State Key Laboratory of High Power Semiconductor Lasers, Changchun University of Science and Technology, Changchun 130022, People's Republic of China

E-mail: ycliu@nenu.edu.cn

Received 21 January 2005, in final form 30 March 2005
Published 29 April 2005
Online at stacks.iop.org/JPhysCM/17/3035

Abstract

Low dimensional (nanowall) ZnO structures were prepared by a two-step growth method with oxygen-plasma-assisted molecular beam epitaxy, where the as-grown film was first engraved on a porous template using the oxygen plasma and then the ZnO nanowalls were grown on the template. The resonance Raman spectra showed the surface mode. A morphology model was proposed on the basis of the scanning electron microscopy patterns and this mode. The room and low temperature photoluminescence showed that the nanowalls had intense ultraviolet emission properties, which benefited from the low dimensional structure with few defects.

1. Introduction

Zinc oxide (ZnO), as a kind of ultraviolet (UV) emission semiconductor material, has attracted considerable research attention in recent years, especially in view of the low dimensional structure of ZnO. In low dimensional structures, charged carriers are confined to certain energy levels, enhancing the exciton oscillator strength and light-emitting efficiency. When the oscillator strength is large enough, nonlinear effects can be observed even under low excitation levels, so the lasing threshold decreases. On the other hand, a low dimensional structure

[4] Author to whom any correspondence should be addressed.

with uniform growth orientation forms natural Fabry–Perot cavities, which make the optical gains rise remarkably [1, 2]. Many efforts have been made to synthesize and characterize low dimension ZnO structure, such as the two-dimensional quantum wells, superlattice structures [3–9] and nanowalls synthesized with carbothermal reduction process [10] and MOCVD [11].

To characterize the low dimensional structure, scanning electron microscopy (SEM) and x-ray diffraction (XRD) are usually used. Raman spectroscopy is another effective method for characterizing the structural properties. For ZnO, group theory predicts the existence of A_1, E_1 and E_2 Raman active modes. The nonpolar E_2 mode characterizes the wurtzite structure of ZnO, while the infrared active modes A_1 and E_1 are split into longitudinal optical phonon (LO) and transverse optical phonon (TO) components, respectively, by the macroscopic electric field. Under backscattering geometry conditions, for *c*-axis preferential growth samples, only the A_1 LO, E_1 TO and nonpolar modes are active, while for polycrystalline samples with random orientation, the A_1 LO, E_1 LO, A_1 TO and E_1 TO modes are all Raman active modes and their superposition forms the LO and TO bands in the Raman spectra [12].

In present work, we report a two-step growth method employing oxygen-plasma-assisted molecular beam epitaxy (P-MBE) for preparing high quality ZnO nanowalls. As reported elsewhere [10, 11], two-dimensional structures with similar morphologies have been prepared with chemical methods. However, the method presented here affords an easier method for controlling growth conditions. Off-resonance Raman and resonance Raman spectra were measured to characterize the low dimensional structure in detail. Room temperature and cryogenic photoluminescence (PL) spectra show that samples prepared by the two-step growth show intense UV emission.

2. Experiment

ZnO nanowalls were prepared using a V80H MBE (VG Company, UK), with a radio-frequency (RF) plasma generator (13.56 MHz, Oxford Company). An electrostatic ion trap (EIT) was used to extract ions and neutral atoms. With the EIT on, only neutral atoms arrived at the substrate, while with the EIT off, both the plasma and the neutral atoms could arrive at the substrate. Hence, the substrate exposure to plasma was controlled during the growth process.

The samples were prepared in a two-step process. Firstly, with the EIT on, ZnO single-crystalline film was grown on Al_2O_3 substrate (approximately 30 nm thickness). Subsequently, with the EIT turned off, the film was bombarded with oxygen plasma for 30 min. Thus, the film surface was engraved to form porous film. The porous film was used as a template for the second step of the growth. With the EIT again on, ZnO was grown on the template in the second step, for 2 h. Comparing with the reported methods [10, 11], in the MBE method it is much easier to control the growth of the nanowalls. In the chemical methods, it is difficult to remove the catalysers, which affects the optical and structural properties.

SEM was performed to characterize the morphology of the ZnO samples. The structural properties were analysed by means of x-ray diffraction (using a D/max-rA XRD spectrometer) and Raman spectra. In the Raman experiments, an Ar^+ laser (488 nm) was used to provide an incident beam in backscattering geometry. A He–Cd laser (325 nm) was chosen as the resonance incident light source because the band gap of ZnO was below this energy at room temperature. PL spectra at room temperature were measured under the same conditions (resonance Raman). Cryogenic PL spectra were also measured to allow analysis of the emission mechanism at temperatures ranging from 80 to 300 K.

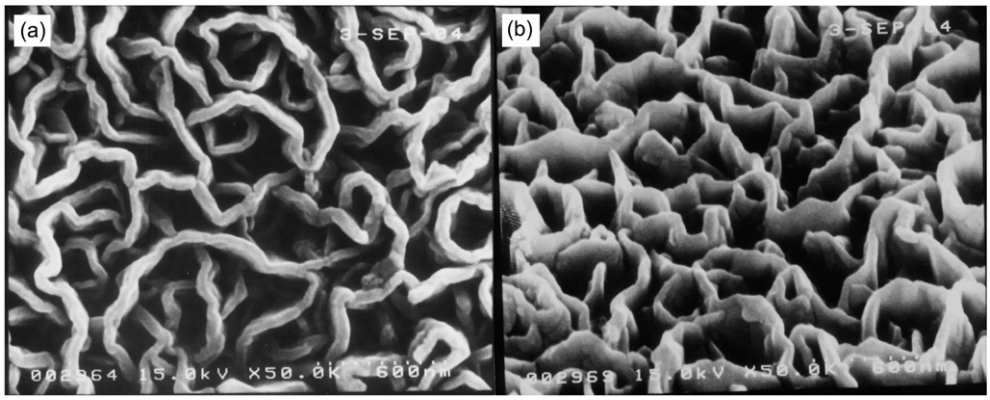

Figure 1. SEM pattern of the samples; (a) is the top view of the nanowalls and (b) is the perspective view pattern.

3. Results and discussion

3.1. Growth and morphology of nanowalls

ZnO nanowalls were obtained through the two-step growth process described above. With the help of RF plasma, the single-crystalline films were engraved to porous structure. Just like for porous silicon, the walls of the holes form low dimensional structures. However, there are large numbers of defects on the surfaces of the nanostructures resulting in a decrease of the UV emission. In order to passivate these defects, the growth process was divided into two steps: (1) a ZnO thin film was grown on Al_2O_3 substrate, and this was followed by RF plasma engraving of the film to produce a random honeycomb-like template; (2) ZnO was grown on the template in the second step. Thus, nanowalls with good crystallinity were obtained. Figure 1 shows typical SEM micrographs, where (a) is a top view of the nanowalls and (b) is the pattern from a viewing angle of 45° relative to the substrate. Two-dimensional ZnO nanowalls are observed as networks with nearly uniform thickness of approximately 80 nm. The walls are serpentine with random curvature on the substrate, with some curving to form irregular rings.

In XRD data, only (002) and (004) peaks can be seen, as shown in figure 2, indicating *c*-axis preferential nanowall growth (the *c*-plane parallel to the substrate). The full width at half-maximum (FWHM) of the ZnO(002) peak is 0.19°. However, it has been reported that the FWHM of (002) XRD peaks are much lower for single-crystalline film [3]. Considering the lattice mismatch, the FWHM is 0.01°–0.02° for growth on the $ScAlMgO_4$ substrate and above 0.04° for growth on the Al_2O_3 substrate. In the present case, the walls are on the nanometre scale, so the size broadening of XRD peaks should be considered. According to the results of SEM, the widths of the walls are 80 nm on average. From the Debye–Scherrer formula: $D = \frac{0.9\lambda}{B\cos\theta_B}$, the ZnO(002) peak (34.4°) corresponds to about 0.2°. Furthermore, the sizes and micrographs of nanowalls are quite similar to those in a recent report [11], in which the nanowalls were grown by chemical methods.

3.2. Raman spectra

The comparison of off-resonance Raman and resonance Raman spectra is shown in figure 3. Curve (a) is the off-resonance Raman spectrum and the curve (b) is the resonance Raman spectrum. The peaks are assigned according to the work of Damen *et al* [13]. The bands

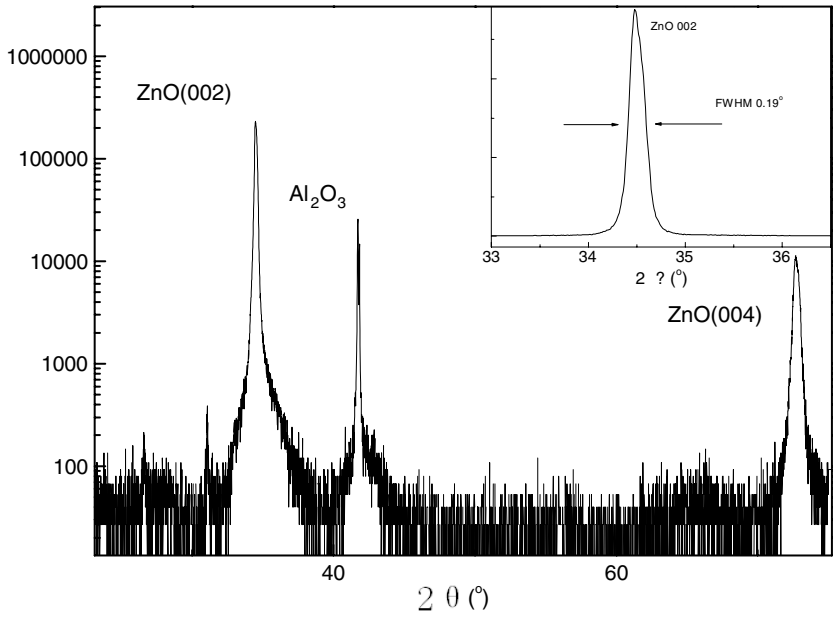

Figure 2. Typical XRD of ZnO nanowalls. Only the (002) and (004) peaks of ZnO can be observed, indicating *c*-axis preferential growth. The inset pattern shows the FWHM of the ZnO(002) peak.

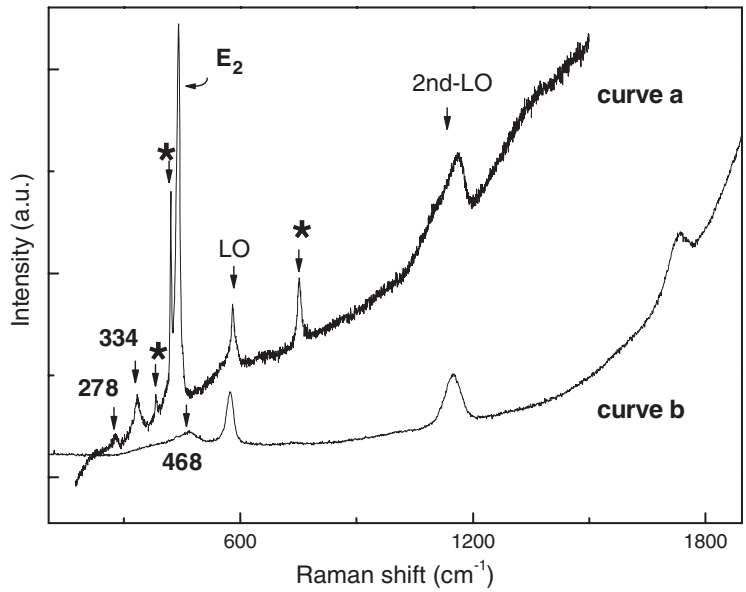

Figure 3. A comparison of off-resonance Raman (curve (a)) and resonance Raman spectra (curve (b)). The peaks marked with * are the substrate Raman signals.

marked with * correspond to the Raman signal from the Al_2O_3 substrate [14, 15]. The peak located at 278 cm^{-1} comes from the local mode of the non-intentional dopant [16–18]. The peak located at 334 cm^{-1} is attributed to a multi-phonon process (E_{2H}–E_{2L}) [13]. The sharp

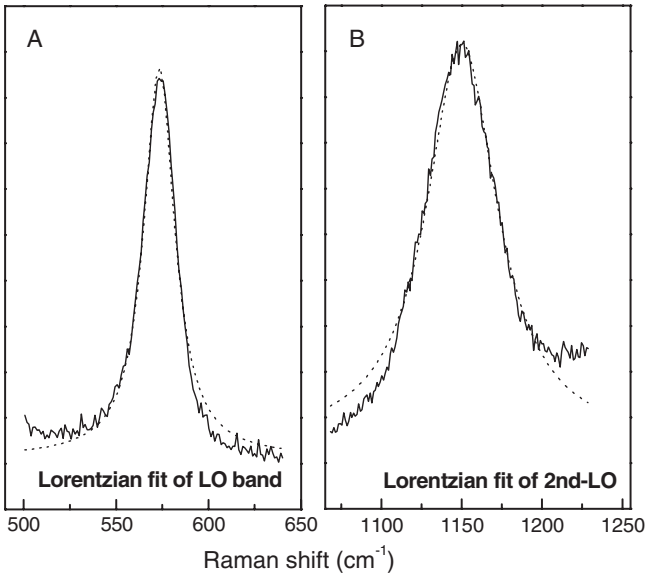

Figure 4. Lorentzian curve fitting of Raman spectra from ZnO nanowalls prepared with MBE. Solid lines are lineshapes of the LO band (A) and second-order LO phonon modes (B); dots show the Lorentzian fit curve.

lineshape of the E_2 mode at 440 cm^{-1} in figure 3 indicates that the nanowalls have wurtzite structure with good crystallinity. In off-Raman spectra the LO band and its overtone are mixed with the substrate signal and elementary excitation. However, since the LO mode is sensitive to the resonance condition, only the LO phonon modes are enhanced in resonance Raman spectra [19]. Thus it can be considered that the LO band in the resonance Raman case is a pure LO mode. The resonance Raman signal of the LO band is located at 574 cm^{-1} and its second-order overtone is located at 1148 cm^{-1}. The Lorentzian curve simulations, as given in figure 4, demonstrate that these two bands have single-Lorentzian lineshape peaks, confirming the *c*-axis preferential growth [12], as indicated by the XRD data.

According to the theory of electromagnetism, charged carrier accumulations at high curvature surfaces and interfaces result in grads of charge distribution, which develop a macroscopic surface electric field. And the surface electric field can interact with excited electrons. Therefore, this interaction gives a contribution to the cross section of Raman scattering with surface or interface modes appearing in the Raman spectra, accordingly. This mechanism is similar to the Frölich interaction, so the surface modes are also enhanced at the resonance condition [19]. The band at 468 cm^{-1} in the resonance Raman spectra in figure 3, curve (b), is assigned to the surface mode for the following reasons: (1) it is located in the region between the TO and LO bands where interface and surface phonon modes are expected [20–22]; (2) the surface mode can be enhanced at the resonance condition [19]; (3) this mode does not have overtones, indicating a local mode rather than an intrinsic mode. This assignment is supported by the results of [16]. In off-resonance Raman spectra the surface mode signal is merged into the E_2 mode. The surface mode is also split into longitudinal (L) and transverse (T) components [20–22]. As shown in figure 3, the only band in the region from the TO mode (407 cm^{-1}) to the LO mode (583 cm^{-1}) is close to the TO mode. So it corresponds to the T component of surface mode and the L component is inexistent, which indicates that the surface electric field is polarized perpendicular to the *c*-axis. On the other hand, the surface

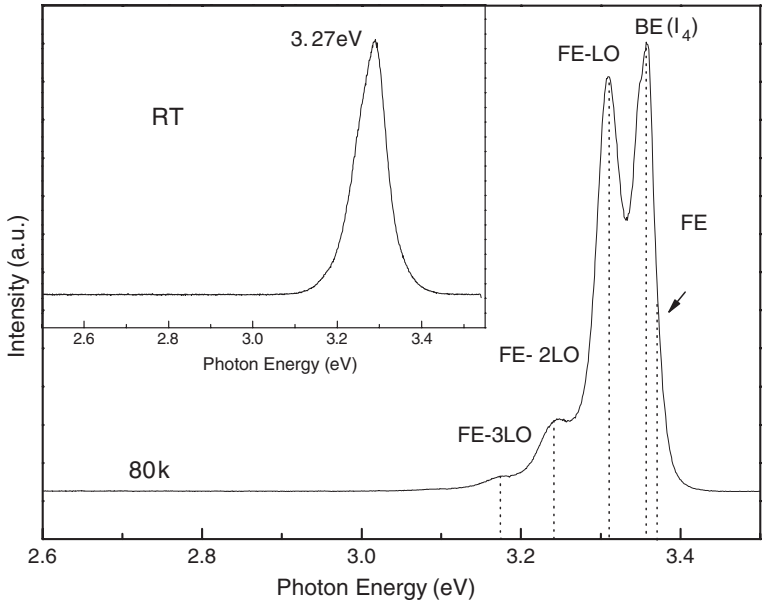

Figure 5. PL spectrum of ZnO nanowalls at 80 K. The inset pattern is the room temperature PL spectrum.

band is broadened and asymmetric, which means that the strength and direction of the surface electric field are irregular. Thus the model of the morphology can be imaged on the basis of the pattern of the surface electric field, which is polarized perpendicular to the *c*-axis with irregular strength and direction. The samples are uniform along the *c*-axis, and the surface parallel to the *c*-axis has random curvature, i.e. nanowalls with serpentine form on the substrate. This result is consistent with the SEM pattern (shown in figure 1).

Furthermore, ZnO is an efficient piezoelectric material. The strain, which mainly comes from the lattice mismatch between the substrate and the ZnO structure, affects the field in the ZnO structure. And the piezoelectric field is one of the factors contributing to the Frölich interaction. However in the nanowall structure, the strain effect of the substrate is relaxed significantly by the several hundred nanometres height [23]. So the electric field affecting the Raman spectra is mostly a surface field.

3.3. Photoluminescence

Figure 5 shows the PL spectrum at 80 K and the inset pattern is the room temperature PL spectrum. It is remarkable that the near-band-edge (NBE) emission (located at 3.27 eV) dominates the room temperature PL pattern, and the deep level (DL) emission is barely observable. The lineshape of the room temperature NBE band is sharp and asymmetric, with a tail on the low energy side. All these properties benefit from the good crystallinity and low dimensional structure. These nanowalls form the Fabry–Perot microcavities, which enhance the optical gain and radiation recombination probability.

There is no significant blue shift of the emission photon energy attributable to the quantum confinement effect in the PL spectra of nanowalls. For the low dimensional structures, the quantum confinement effect usually affects the oscillator strengths of exciton recombination, exciton binding energy and quantization energy ΔE. As the structure size decreases, these

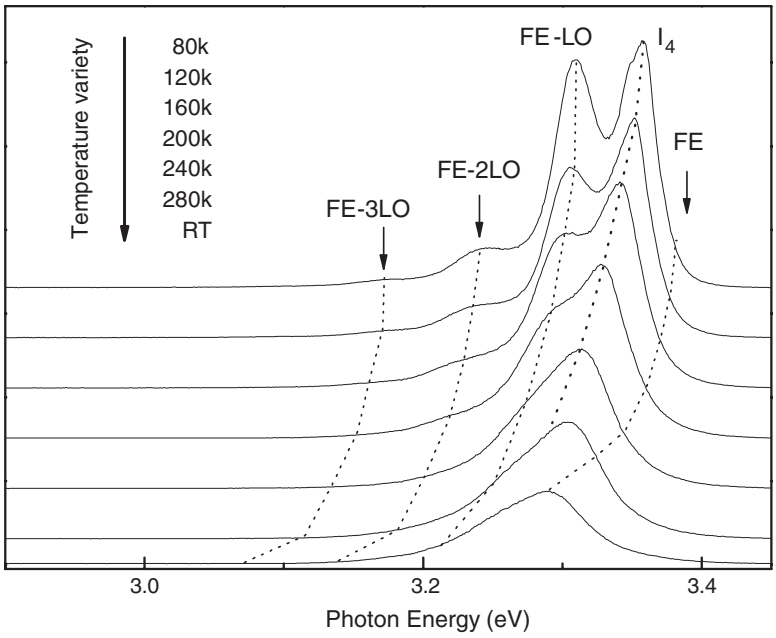

Figure 6. PL spectra of ZnO nanowalls over the temperature range 80 K to ∼300 K.

three factors increase. However, the quantum confinement effect affects the photon emission energy in two respects. Although both the ΔE and the exciton binding energy increase with decrease of the dimensional size, they make opposite contributions. In general, ΔE makes the emission band blue shift, while the exciton binding energy makes the emission band red shift. In fact, the quantum confinement effect will be observed only when the scale of the confined direction is similar to the scale of the exciton Bohr radius (a_B). In bulk ZnO, the exciton Bohr radius is $a_B \sim 2.34$ nm. That is to say, the confined size should be smaller than several nanometres. These quantum confinement phenomena have been demonstrated for quantum wells and superlattices [5–8]. Furthermore, well width dependence of the exciton resonance energy has been reported [9]. In the nanowalls, however, the scale of crystal grains is 80 nm on average. Therefore, there is no significant blue shift according to the quantum confinement effect in the PL spectra.

In the cryogenic PL spectra the strongest band, located at 3.358 eV, is I_4; the binding energy of the exciton bound to neutral donors is about 13 meV [24]. The higher energy side shoulder of I_4 is assigned to the free exciton, with three phonon replicas observed at 3.309, 3.240 and 3.169 eV. As temperature increases, I_4 decreases in intensity, thermally releasing excitons from the donor impurities. With further increase in temperature, free exciton emission occurs and eventually dominates the PL spectra, as shown in figure 6. At 280 K, the bound exciton was completely thermally ionized. The phonon replicas contribute to the lower energy side of the room temperature NBE emission.

4. Conclusions

High quality ZnO nanowalls were prepared by a two-step growth method with P-MBE. SEM shows nanowalls with uniform thickness and irregular curvature. The comparison of off-

resonance Raman and resonance Raman spectra shows a surface mode and a mode induced by the surface electric field, indicative of morphology consistent with the SEM pattern. The room temperature PL indicates high efficiency UV emission, while the cryogenic PL shows that the primary emission is from bound and free exciton recombination. The superior optical and structural properties of the nanowalls produced by this growth method may be applied in the manufacturing industries for producing solar cells, sensors and light-emitting devices. And the comparison of off-resonance Raman and resonance Raman spectra can be used as a convenient method to characterize this special morphology.

Acknowledgments

This work was supported by the National Natural Science Foundation of China, No. 60376009, 60278031, the Major Project of the National Natural Science Foundation of China, No. 60336020, and the Cultivation Fund of the Key Scientific and Technical Innovation Project, Ministry of Education of China, No. 704017.

References

[1] Segawa Y 1997 *Phys. Status Solidi* b **202** 669
[2] Tang Z K, Wong G K L and Yu P 1998 *Appl. Phys. Lett.* **72** 3270
[3] Ohtomo A, Tamura K, Saikusa K, Takahashi K, Makino T, Segawa Y, Koinuma H and Kawasaki M 1999 *Appl. Phys. Lett.* **75** 2635
[4] Look D C, Reynolds D C, Litton C W, Jones R L, Eason D B and Cantwel G 2002 *Appl. Phys. Lett.* **81** 1830
[5] Matsui H, Saeki H, Tabata H and Kawai T 2003 *Japan. J. Appl. Phys.* **42** 5494
[6] Ohtomo A, Kawasaki M, Ohkubo I, Koinuma H, Yasuda T and Segawa Y 1999 *Appl. Phys. Lett.* **75** 980
[7] Makino T, Chia C H, Tuan Nguen T, Sun H D, Segawa Y, Kawasaki M, Ohtomo A, Tamura K and Koinuma H 2000 *Appl. Phys. Lett.* **77** 975
[8] Chia C H, Makino T, Segawa Y, Kawasaki M, Ohtomo A, Tamura K and Koinuma H 2001 *J. Appl. Phys.* **90** 3650
[9] Gruber T, Kirchner C, Kling R, Reuss F and Waag A 2004 *Appl. Phys. Lett.* **84** 5359
[10] Ng H T, Li J, Smith M K, Nguyer P, Cassell A, Han J and Meyyappan M 2003 *Science* **300** 1249
[11] Zhang B P, Wakatsuki K, Binh N T and Segawa Y 2004 *J. Appl. Phys.* **96** 340
[12] Arguello C A, Rousseau D L and Porto S P S 1969 *Phys. Rev.* **181** 1351
[13] Danmen T C, Porto S P S and Tell B 1966 *Phys. Rev.* **142** 570
[14] Kadleikova M, Breza J and Vesely M 2001 *Microelectron. J.* **32** 955
[15] Schubert M, Tiwald T E and Herzinger C M 2000 *Phys. Rev.* B **61** 8187
[16] Tzolov M, Tzenov N, Dimova-Malinovska D, Kalitzova M, Pizzuto C, Vitali G, Zollo G and Ivanov I 2000 *Thin Solid Film* **379** 28
[17] Kaschner A, Haboeck U, Strassburg M, Strassburg M, Kaczmarczyk G, Hoffmann A, Thomsen C, Zeuner A, Alves H R, Hofmann D M and Meyer B K 2002 *Appl. Phys. Lett.* **80** 1909
[18] Bundesmann C, Ashkenov N, Schubert M, Spemann D, Butz T, Kaidashev E M, Lorenz M and Grundmann M 2003 *Appl. Phys. Lett.* **83** 1974
[19] Cardona M and Guntherodt G 1983 *Light Scattering in Solids* 2nd edn (Berlin: Springer)
[20] Yamamoto K, Tran C D, Abe K and Shimizu H 1977 *J. Phys. Soc. Japan* **42** 587
[21] Yamamoto K, Ueda K, Yamada M and Abe K 1979 *J. Phys. Soc. Japan* **46** 1792
[22] Hayashi S, Nakamori N and Kanamori H 1979 *J. Phys. Soc. Japan* **46** 176
[23] Zhang Y, Jia H, Wang R, Chen C, Luo X, Yu D and Lee C 2003 *Appl. Phys. Lett.* **83** 4631
[24] Meyer B K, Alves H, Hofmann D M, Kriegseis W, Forster D, Bertram F, Christen J, Hoffmann A, Straßburg M, Dworzak M, Haboeck U and Rodina A V 2004 *Phys. Status Solidi* b **241** 231